Enhancement and Quenching of Single-Molecule Fluorescence

Pascal Anger, Palash Bharadwaj, and Lukas Novotny*

The Institute of Optics and Department of Physics and Astronomy, University of Rochester, Rochester, New York 14627, USA†

(Received 23 November 2005; published 21 March 2006)

We present an experimental and theoretical study of the fluorescence rate of a single molecule as a function of its distance to a laser-irradiated gold nanoparticle. The local field enhancement leads to an increased excitation rate whereas nonradiative energy transfer to the particle leads to a decrease of the quantum yield (quenching). Because of these competing effects, previous experiments showed either fluorescence enhancement or fluorescence quenching. By varying the distance between molecule and particle we show the first experimental measurement demonstrating the continuous transition from fluorescence enhancement to fluorescence quenching. This transition cannot be explained by treating the particle as a polarizable sphere in the dipole approximation.

DOI: 10.1103/PhysRevLett.96.113002 PACS numbers: 33.50.−j, 68.37.Uv, 73.20.Mf, 78.67.Bf

Since the pioneering work of Purcell it is well known that the lifetime of an excited atomic state is not only a function of the atom but also of its environment [1]. Purcell's prediction has been verified in different experimental settings such as close to plane interfaces [2,3], in cavities [4] and photonic crystals [5], and close to near-field optical probes [6]. It was realized that the modification of the lifetime is influenced by the radiative decay rate due to photon emission and by the nonradiative decay rate due to energy dissipation in the environment [3,6,7]. For atoms or molecules close to metal surfaces both rates can be enhanced [8–10]. Excited-state lifetimes of single molecules have been measured as a function of their separation from laser-irradiated metal boundaries and satisfactory agreement with theory has been achieved [3,6,11]. However, the results related to the fluorescence rate are *not* consistent. While some studies demonstrate fluorescence enhancement for a molecule placed near a metal nanostructure [12,13], other studies report fluorescence quenching [14,15]. The problem originates from the fact that fluorescence is the product of two processes: (1) Excitation by the incident field influenced by the local environment, and (2) emission of radiation influenced by the balance of radiative and nonradiative decay. While the source of process (1) is the external radiation field, in process (2) it is the molecule itself which constitutes the source [10,16].

In this Letter, we investigate the fluorescence rate of a single molecule as a function of its separation from a laser-irradiated, spherical gold nanoparticle. This configuration is chosen because it allows for a quantitative comparison with theoretical calculations. We achieve almost perfect agreement without using any adjustable parameters. A quantitative understanding of single-molecule fluorescence in inhomogeneous environments is important for the development of nanoscale sensors and biomolecular assays [14,17], for the developing field of nanoplasmonics [18], and for the emerging concept of optical antennas employed in surface enhanced spectroscopy and microscopy [19–24].

Let us consider a single molecule located at $\mathbf{r}_m$ and represented by a two-level system with transition dipole moment $\mathbf{p}$ and transition frequency ω. For weak excitation (no saturation), the fluorescence rate γ_{em} is a two-step process which involves the excitation rate γ_{exc} and the emission probability represented by the quantum yield $q_a = \gamma_r/\gamma$, with γ_r and γ being the radiative decay rate and the total decay rate, respectively. In principle, γ_{exc} has to be evaluated at the excitation frequency and q_a at the emission frequency. However, because we excite the molecules at the peak of their emission spectrum, a single-frequency approximation is justified. The fluorescence rate can then be written as

$$\gamma_{\mathrm{em}} = \gamma_{\mathrm{exc}}[\gamma_r/\gamma] = \gamma_{\mathrm{exc}}[1 - (\gamma_{\mathrm{nr}}/\gamma_0)/(\gamma/\gamma_0)], \quad (1)$$

where γ_0 is the free-space decay rate, $\gamma_{\mathrm{nr}} = \gamma - \gamma_r$ is the nonradiative decay rate and $\gamma_{\mathrm{exc}} \propto |\mathbf{p}\cdot\mathbf{E}|^2$ is the excitation rate depending on the local excitation field $\mathbf{E}(\mathbf{r}_m, \omega)$.

Based on Fermi's golden rule, the spontaneous decay rate γ can be expressed as (SI units)

$$\gamma = \frac{2\omega}{3\hbar\varepsilon_0}|\mathbf{p}|^2\rho(\mathbf{r}_m, \omega), \quad (2)$$

where ω is the transition frequency and ρ denotes the electromagnetic density of states. The latter can be expressed in terms of the system's dyadic Green's function $\overleftrightarrow{\mathbf{G}}$ as [25,26]

$$\rho(\mathbf{r}_m, \omega) = \frac{6\omega}{\pi c^2}[\mathbf{n}_p \cdot \mathrm{Im}\{\overleftrightarrow{\mathbf{G}}(\mathbf{r}_m, \mathbf{r}_m\} \cdot \mathbf{n}_p], \quad (3)$$

where $\mathbf{n}_p$ is a unit vector pointing in direction of $\mathbf{p}$. Thus, the decay rate of a molecule is determined by the Green's function of the system in which the molecule is embedded. In free space we obtain $\rho = \omega^2/(\pi^2 c^3)$ and $\gamma_0 = \omega^3|\mathbf{p}|^2/(3\pi\varepsilon_0\hbar c^3)$.

We assume that the molecule has a high intrinsic quantum yield and that the nonradiative rate is determined by Ohmic losses in the environment according to [3]

$$\frac{\gamma_{\rm nr}}{\gamma_0} = \frac{1}{P_0}\frac{1}{2}\int_V {\rm Re}\{\mathbf{j}(\mathbf{r})\cdot\mathbf{E}_m^*(\mathbf{r})\}d\mathbf{r}^3, \qquad (4)$$

which follows from a simple energy balance. Here, $P_0 = \omega^4|\mathbf{p}|^2/(12\pi\varepsilon_0 c^3)$ denotes the power emitted by a classical dipole, $\mathbf{j}$ is the induced current density restricted to finite regions V in the environment, and $\mathbf{E}_m$ is the field emitted by the molecule which can be written in terms of the Green's function introduced earlier as $\mathbf{E}_m(\mathbf{r}) = (k^2/\varepsilon_0)\vec{\mathbf{G}}(\mathbf{r},\mathbf{r}_m)\mathbf{p}$, where $k = \omega/c$. The current density can be expressed in terms of the molecular field as $\mathbf{j} = \omega\varepsilon_0\varepsilon''\mathbf{E}_m$, with ε'' being the imaginary part of the dielectric constant. Equations (2) and (4) determine the quantum yield q_a of the molecule.

In the absence of any objects in the environment, the molecule is excited by the incident radiation field $\mathbf{E}_0$. The interaction of $\mathbf{E}_0$ with the environment gives rise to a secondary field that can, for example, be calculated by solving a volume integral equation using the system's Green's function $\vec{\mathbf{G}}$. Assuming that the environment does not affect the molecule's polarizability the normalized excitation rate can be expressed as

$$\gamma_{\rm exc}/\gamma_{\rm exc}^0 = |[\mathbf{n}_p\cdot\mathbf{E}(\mathbf{r}_m)]/[\mathbf{n}_p\cdot\mathbf{E}_0(\mathbf{r}_m)]|^2, \qquad (5)$$

where $\gamma_{\rm exc}^0$ is the excitation rate in free space and $\mathbf{E}$ is the total local field (incident plus scattered). We have now all ingredients to calculate the fluorescence rate $\gamma_{\rm em}$ in Eq. (1). The result depends on $\mathbf{E}_0$, $\mathbf{n}_p$, and the properties of the environment encoded in $\vec{\mathbf{G}}$ and $\varepsilon(\mathbf{r})$.

Let us consider a molecule interacting with a single spherical gold nanoparticle of diameter d. The distance between molecule and particle center is $z + d/2$, and the axis connecting molecule and particle center is denoted as the z axis. The system is irradiated by a plane wave polarized along the z axis. For a small particle ($d \ll \lambda$) the scattered field along the z axis will also be z polarized and therefore molecules oriented perpendicular to the z axis will not be excited. Furthermore, for such molecule orientations there is no enhancement of the radiative decay rate [9]. It therefore suffices to consider molecules oriented along the z axis. We have applied two different methods to solve for the different rates: (1) The multiple multipole (MMP) method [26], and (2) the dipole approximation [9]. For both methods, Fig. 1 shows the calculated rates as a function of the separation z. The dipole approximation is only valid if $d \ll \lambda$ *and* if the exciting field is homogeneous across the dimensions of the particle. Obviously, the latter requirement is violated if the nanoparticle is excited by a molecule placed in close proximity and hence the dipole approximation yields an erroneous result for q_a and $\gamma_{\rm em}$.

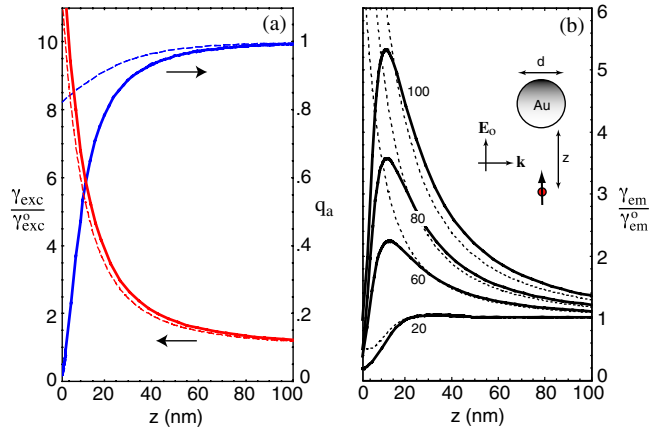

FIG. 1 (color online). Calculated quantum yield q_a, excitation rate $\gamma_{\rm exc}$, and fluorescence rate $\gamma_{\rm em}$ as a function of molecule-particle separation. $\gamma_{\rm exc}$ and $\gamma_{\rm em}$ are normalized with their corresponding free-space values ($z \to \infty$). The solid curves are the result of MMP calculations (max. error 2%) whereas the dashed curves correspond to the dipole approximation which fails for short distances z. In (a) the particle diameter is $d =$ 80 nm and in (b) it is indicated in the figure. Excitation wavelength is $\lambda = 650$ nm and $\varepsilon = -12.99 + i1.09$ (gold).

In the dipole approximation, the particle is treated as a polarizable dipolar entity giving rise to the following expression for the system's Green's function [26]

$$\vec{\mathbf{G}}(\mathbf{r},\mathbf{r}_m) = \vec{\mathbf{G}}^0(\mathbf{r},\mathbf{r}_m) + \frac{k^2}{\varepsilon_0}\vec{\mathbf{G}}^0(\mathbf{r},\mathbf{r}_0)\vec{\alpha}_{\rm eff}\vec{\mathbf{G}}^0(\mathbf{r}_0,\mathbf{r}_m), \qquad (6)$$

where $\vec{\mathbf{G}}^0$ is the free-space Green's dyadic and $\mathbf{r}_0$ denotes the particle origin. The effective polarizability $\alpha_{\rm eff}$ is defined as [9,24]

$$\vec{\alpha}_{\rm eff} = \vec{\alpha}[\vec{\mathbf{I}} - ik^3/(6\pi\varepsilon_0)\vec{\alpha}]^{-1} \qquad (7)$$

with $\vec{\alpha} = (\pi/2)\varepsilon_0 d^3\vec{\mathbf{I}}(\varepsilon - 1)/(\varepsilon + 2)$ denoting the quasistatic polarizability and $\vec{\mathbf{I}}$ the unit dyad. The second term in Eq. (7) arises from radiation reaction, i.e., the action of the particle on itself. Without this term, the optical theorem is violated. With the help of $\vec{\mathbf{G}}(\mathbf{r},\mathbf{r}_m)$ we can calculate the different decay rates γ, $\gamma_{\rm nr}$, and γ_r.

The molecule's local excitation field $\mathbf{E}(\mathbf{r}_m)$ can be expressed in terms of the free-space Green's function as

$$\mathbf{E}(\mathbf{r}_m) = \mathbf{E}_0(\mathbf{r}_m) + \frac{k^2}{\varepsilon_0}\vec{\mathbf{G}}^0(\mathbf{r}_m,\mathbf{r}_0)\vec{\alpha}_{\rm eff}\mathbf{E}_0(\mathbf{r}_m), \qquad (8)$$

which can be introduced into Eq. (5) to yield the normalized excitation rate in the dipole approximation.

While the excitation rate is reasonably well described by the dipole approximation, the quantum yield is not [cf. Fig. 1(a)]. The dipole approximation strongly overestimates the quantum yield at short distances and does not predict any fluorescence quenching [cf. Fig. 1(b)]. Higher multipole orders are needed for a more accurate descrip-

tion of the nonradiative rate in Eq. (4). The MMP calculation shows that, for short distances, the decrease of quantum yield wins over the increase of the excitation rate thereby quenching the fluorescence of the molecule. Our study also revealed that maximum fluorescence enhancement is obtained for excitation frequencies redshifted from the surface plasmon resonance of the particle (data not shown) consistent with the predictions of Ref. [8]. Fluorescence enhancement is strongest for $\lambda \approx 680$ nm and weakest for $\lambda \approx 485$ nm.

To test the theoretical predictions we carried out the experiment schematically shown in Fig. 2(a). Single-molecule samples were prepared by spin coating a 1 nM solution of nile blue on a cleaned glass coverslip. The sample was then overcoated with a thin layer (20 or 2 nm) of polymethyl methacrylate (PMMA). The thickness was determined by razor-blade scratching and subsequent imaging with atomic force microscopy (AFM). Spin casting of the PMMA layer resulted in molecules with different out-of-plane dipole orientations. A microscope objective with NA = 1.4 was used to focus a radially polarized laser beam with wavelength $\lambda = 637$ nm on the sample surface. Confocal fluorescence rate images were acquired by raster scanning the sample in the focal plane of the laser beam and recording the fluorescence rate for each image pixel. The fluorescence rate patterns allowed us to identify molecules with vertical dipole moments (oriented perpendicular to sample surface) [27]. A spherical gold nanoparticle with diameter $d = 80$ nm was attached to the end of a pointed optical fiber [28] as shown by the SEM image in the inset of Fig. 2(a). The supporting fiber was attached to a tuning-fork crystal whose resonance frequency was used in a feedback loop to maintain a constant distance z. Finally, the attached gold particle was positioned into the center of the laser focus by maximizing the backscattered light from the gold particle. Near-field fluorescence images were obtained by raster scanning the sample while maintaining a constant particle-sample separation. Distance curves of the fluorescence rate were recorded by positioning the gold particle over a previously determined, vertically oriented molecule and recording the emission rate as a function of particle-sample distance.

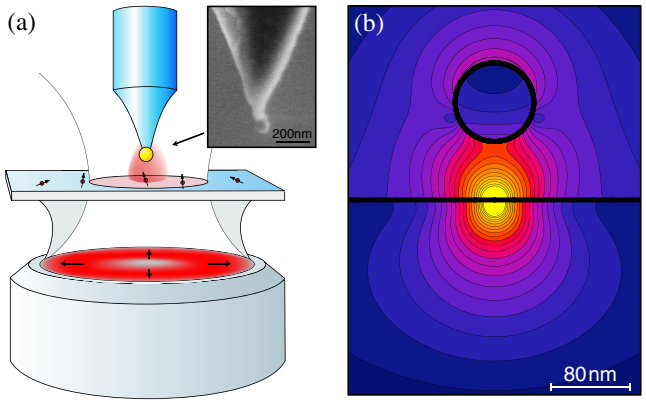

FIG. 2 (color online). (a) Sketch of the experimental arrangement. See text for details. Inset: SEM image of a gold particle attached to the end of a pointed optical fiber. (b) Field distribution ($|\mathbf{E}|^2$, factor of 2 between successive contour lines) of an emitting dipole ($\lambda = 650$ nm) located 2 nm underneath the surface of a glass substrate and faced by a gold particle separated by a distance of $z = 60$ nm from the glass surface.

The experimental configuration differs from the previous model by the supporting glass cover slip and by the different excitation source used. Therefore, the MMP calculations were repeated for a vertical molecule embedded in a dielectric substrate ($\varepsilon_s = 2.25$) and excited by a radially polarized focused laser beam. Figure 2(b) shows the calculated field distribution resulting from a classically emitting molecule located 2 nm underneath the surface and faced by a 80 nm gold particle. Calculations of the quantum yield had to take into account that only photons emitted into the lower half-space were detected. In the absence of the gold particle this amounts to 85% of the total radiation. This value varies by less than 5% as a function of molecule-particle separation z.

Figure 3 shows fluorescence rate images of a single-molecule sample. In (a) the gold particle was removed resulting in a confocal fluorescence image with diffraction limited resolution. When excited by a radially polarized beam, most molecules exhibit a double-lobed pattern [27]. The outlined section in (a) was reimaged with the gold particle held at a distance of $z \approx 5$ nm and the result is shown in Fig. 3(b). The shape and intensity of individual fluorescence spots varies in the image because the sample consists of molecules with different dipole orientations. The thickness of the overcoating PMMA layer was 20 nm and no fluorescence quenching was observed. Therefore, in a second round of experiments, the PMMA thickness was reduced to 2 nm.

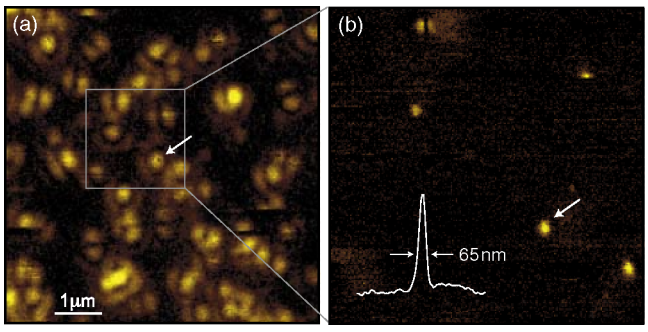

FIG. 3 (color online). Fluorescence rate images of a sample of nile blue molecules. (a) Confocal image using a radially polarized excitation beam. (b) Near-field image of the marked area exploiting the local field enhancement at a gold nanoparticle ($d = 80$ nm) positioned into the laser focus ($z = 5$ nm). The arrows mark a vertically oriented molecule. The inset shows a cross section through the indicated near-field spot. In (b), the laser power has been attenuated by a factor of 3.2.

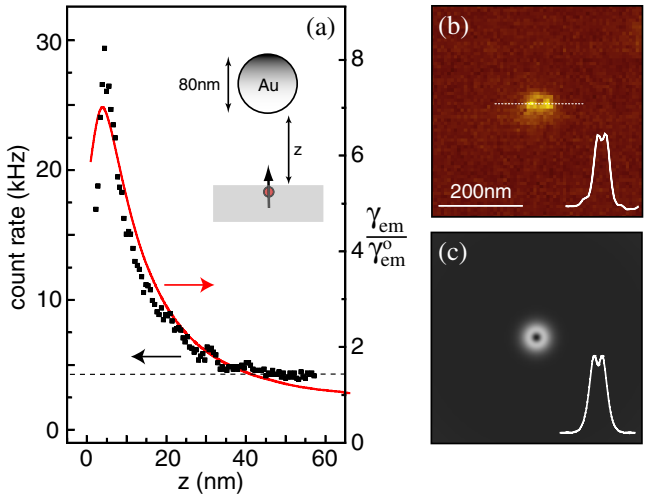

FIG. 4 (color online). (a) Fluorescence rate as a function of particle-surface distance z for a vertically oriented molecule (solid curve: theory, dots: experiment). The horizontal dashed line indicates the background level. (b) Fluorescence rate image of a single molecule acquired for $z \approx 2$ nm. The dip in the center indicates fluorescence quenching. (c) Corresponding theoretical image.

Figure 4(a) shows the fluorescence rate of a vertically oriented molecule as a function of particle-sample distance z. Experimental data (dots) are shown together with the theoretical curve derived from MMP calculations [cf. Fig. 2(b)]. No adjustable parameters are used in this calculation and the agreement between theory and experiment is surprisingly good. The fluorescence enhancement reaches a maximum at a distance of $z \approx 5$ nm. For shorter distances fluorescence is quenched. In the experiments, the fluorescence background is $\approx$4 kHz and originates from different sources such as gold luminescence. The background changes slightly with distance z, which is likely the reason for the slight deviation between theory and experiment. Other sources of error are calibration tolerances and the fact that the molecule's orientation is not perfectly vertical. Interestingly, for distances $z < 2$ nm the measured fluorescence rate drops more rapidly than the theoretical curve which is indicative for nonlocal effects (failure of local dielectric constants) and other surface related effects such as contamination. In Fig. 4(b) we show a typical fluorescence rate image of a vertically oriented molecule acquired at $z \approx 2$ nm. The molecule shows up as a donut pattern due to fluorescence quenching in the center of the image [21]. As shown in Fig. 4(c), the same pattern is predicted by our calculations. We have repeated the experiments for a different excitation wavelength of $\lambda = 532$ nm and a different molecule (DiI). The results are consistent with the findings reported in this Letter.

In conclusion, we have quantitatively measured the continuous transition from fluorescence enhancement to fluorescence quenching on a single molecule. Our results are important for the understanding, prediction, and control of photophysical processes on the nanometer scale, particularly for the development of nanoscale sensors, biomolecular assays, nanoplasmonic devices, and for the development of novel optical antennas employed in surface enhanced spectroscopy and microscopy.

We are very grateful to Shanlin Pan and Lewis Rothberg for assistance with surface chemistry. This work was supported by the Department of Energy under Grant No. DE-FG02-01ER15204.

*Corresponding author.
Electronic address: novotny@optics.rochester.edu
†Electronic address: http://www.nano-optics.org

[1] E. M. Purcell, Phys. Rev. **69**, 681 (1946).
[2] K. H. Drexhage, Prog. Opt. **12**, 163 (1974).
[3] R. R. Chance, A. Prock, and R. Silbey, Adv. Chem. Phys. **37**, 1 (1978).
[4] D. Kleppner, Phys. Rev. Lett. **47**, 233 (1981).
[5] P. Lodahl *et al.*, Nature (London) **430**, 654 (2004).
[6] R. X. Bian *et al.*, Phys. Rev. Lett. **75**, 4772 (1995).
[7] L. Novotny, Appl. Phys. Lett. **69**, 3806 (1996).
[8] M. Thomas *et al.*, Appl. Phys. Lett. **85**, 3863 (2004).
[9] R. Carminati *et al.*, Opt. Commun. (to be published).
[10] J. N. Farahani *et al.*, Phys. Rev. Lett. **95**, 017402 (2005).
[11] B. C. Buchler *et al.*, Phys. Rev. Lett. **95**, 063003 (2005).
[12] K. T. Shimizu *et al.*, Phys. Rev. Lett. **89**, 117401 (2002).
[13] A. Kramer *et al.*, Appl. Phys. Lett. **80**, 1652 (2002).
[14] E. Dulkeith *et al.*, Nano Lett. **5**, 585 (2005).
[15] W. Trabesinger *et al.*, Appl. Phys. Lett. **81**, 2118 (2002).
[16] J. T. Krug II, E. J. Sanchez, and X. S. Xie, Appl. Phys. Lett. **86**, 233102 (2005).
[17] M. J. Levene *et al.*, Science **299**, 682 (2003).
[18] *Synthesis and Plasmonic Properties of Nanostructures*, edited by Y. Xia and N. J. Halas [MRS Bull. 30, 338 May (2005)].
[19] R. Grober, R. Schoellkopf, and D. Prober, Appl. Phys. Lett. **70**, 1354 (1997).
[20] F. Keilmann and R. Hillenbrand, Phil. Trans. R. Soc. Lond. A **362**, 787 (2004).
[21] H. G. Frey *et al.*, Phys. Rev. Lett. **93**, 200801 (2004).
[22] P. Mühlschlegel *et al.*, Science **308**, 1607 (2005).
[23] P. J. Schuck *et al.*, Phys. Rev. Lett. **94**, 017402 (2005).
[24] T. Kalkbrenner *et al.*, Phys. Rev. Lett. **95**, 200801 (2005).
[25] K. Joulain *et al.*, Phys. Rev. B **68**, 245405 (2003).
[26] L. Novotny and B. Hecht, *Principles of Nano-Optics* (Cambridge University Press, Cambridge, England, 2006).
[27] L. Novotny *et al.*, Phys. Rev. Lett. **86**, 5251 (2001).
[28] T. Kalkbrenner *et al.*, J. Microsc. **202**, 72 (2001).